THE JOURNAL OF PHYSICAL CHEMISTRY C

ARTICLE

pubs.acs.org/JPCC

Enhanced Nucleation and Growth of Diamond Film on Si by CVD Using a Chemical Precursor

Rajanish N. Tiwari,*[,†,§] Jitendra N. Tiwari,[‡] Li Chang,[§] and M. Yoshimura[†]

[†]Surface Science Laboratory, Toyota Technological Institute, 2-12-1 Hisakata Tempaku, Nagoya 468-8511, Japan

[‡]Center for Superfunctional Materials, Department of Chemistry, Pohang University of Science and Technology, San 31, Hyojadong, Namgu, Pohang 790-784, Korea

[§]Department of Materials Science and Engineering, National Chiao Tung University, 1001 Ta Hsueh Road, Hsinchu, Taiwan, 30050, R.O.C.

ABSTRACT: Nucleation of diamond is of great importance for its growth, and a detailed understanding of the nucleation process is, therefore, desired for many applications. The pretreatment of the substrate surface may impact the initial growth period. This study demonstrates the synthesis of diamond films by microwave plasma chemical vapor deposition on a Pt/SiO_2/Si substrate. The Pt particles were deposited on the SiO_2/Si surface at room temperature, whereas adamantane was seeded on the SiO_2/Si surface by ultrasonic treatment. The Pt particles on the SiO_2 surface behave as a catalyst, which adsorb hydrocarbons from adamantane contained plasma and give distinct features of carbon in the early stage deposition. The adamantane transforms not only in the nanodiamond phase but also in other carbon phases, which can then act as nuclei for diamond growth. These kinds of phases enhanced the diamond density at partially low temperature deposition. The presence of an oxide intermediate layer between Pt and Si prevents silicidation as well as SiC in diamond deposition.

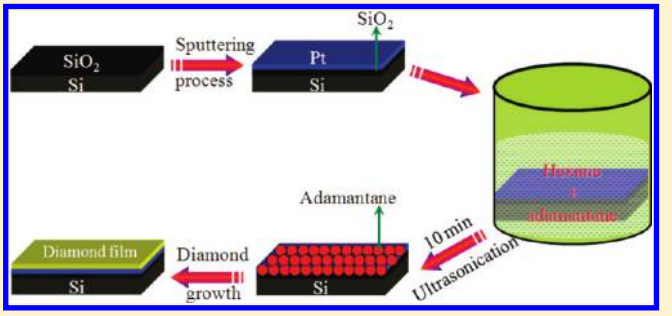

1. INTRODUCTION

Diamond has a variety of outstanding properties, such as wide band gap, chemical inertness, high carrier mobility, excellent biological compatibility, high propagation speed of acoustic wave, good optical transparency, high thermal conductivity, and the greatest hardness, which make it a promising candidate for a wide range of applications, for instance, microelectronics, optics, tribological, thermal management, biomedical, DNA-based sensors, manufacturing engineering, and so on.[1−7] Platinum has been used as a substrate for the growth of chemical vapor deposited (CVD) diamond film. Recently, platinum (Pt) is used for high-pressure, high-temperature diamond synthesis as a catalytic solvent.[8] It is also known that Pt is a strong catalyst for hydrogen and hydrocarbons. Therefore, there is definite interest in studying the effects of Pt on diamond growth. The lattice constant of diamond and platinum (*fcc*) is 3.56 and 3.92 Å, respectively. Therefore, the lattice difference between diamond and Pt is approximately ∼10%.[9] Tachibana et al. have studied diamond growth on Pt substrate by a bias-enhanced nucleation method. They had noticed that the density of diamond nucleation was enhanced with bias time.[10] Most recently, the growth of diamond films on a Pt layer was realized by microwave plasma chemical vapor deposition (MPCVD) without bias treatment. In this technique, they used diamond seeding particles to enhance the diamond nucleation.[11] Although diamond films on a Pt/non-Si substrate, for example, single-crystal $SrTiO_3$ (111) or sapphire substrates have been studied.[12,13] However, very few studies of diamond growth on a Pt/Si substrate have been reported at partially low temperature. The prevention of silicidation is the key to growing high-quality diamond on Pt/Si.

In this paper, we report for the first time chemical vapor deposition of diamond films on Pt/SiO_2/Si by using adamantane as a seeding layer to enhance the diamond nucleation at partially low temperature. Adamantane ($C_{10}H_{16}$) is one of a series of carbon structures, a very stable crystalline compound, and a highly symmetric molecule with point group symmetry, T_d. Adamantane is the smallest possible diamondoid (chemical formula $C(4n + 6)H(4n + 12)$, where $n = 0, 1, 2, 3...$), consisting of 10 carbon atoms arranged as a single diamond cage surrounded by 16 hydrogen atoms.[14−16] A cagelike structure is formed with six CH_2 and four CH groups giving rise to a molecular structure with four cyclohexane rings in chair form. Its structure has zero strain as all C−C−C bond angles are 109.45° with a corresponding bond length of 1.54 Å, and the C−H bond length is 1.1 Å. The density of adamantane is 1.07 g/cm^3. Adamantane does not melt at ambient pressure but sublimates. Adamantane can sublime easily and has a relatively high vapor pressure. Partial breakdown of adamantane is known to yield

Received: May 4, 2011
Revised: June 21, 2011
Published: July 05, 2011

dx.doi.org/10.1021/jp2041179 | *J. Phys. Chem. C* 2011, 115, 16063–16073

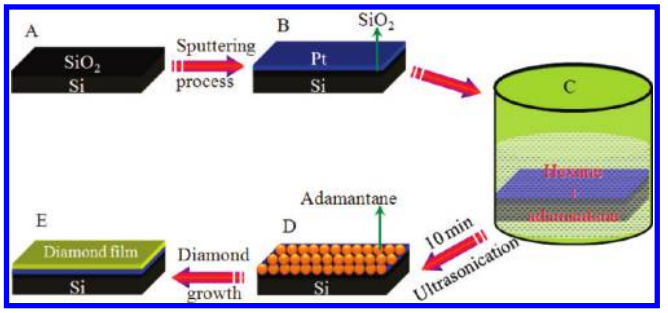

Figure 1. Schematic diagram showing diamond synthesis in five steps: (a) silicon substrate with native oxide layer, (b) Pt coated on the SiO_2/Si substrate by a sputtering process, (c) Pt/SiO_2/Si immersed into the hexane + adamantane solution, (d) adamantane deposited on the Pt/SiO_2/Si surface by ultrasonication, and (e) diamond growth by MPCVD.

carbon clusters (C_nH_x), where $n = 3, 5, 6, 7, 8$, and 9, of significant abundance.[17,18] In addition, adamantane easily dissolves in organic solvents and is widely commercially available. Therefore, in this study, we used hexane (C_6H_{14}) as a solvent. The evaporation properties of hexane are high. After adamantane is seeded on the Pt/Si surface by ultrasonication, the hexane will be evaporated from the Si surface and only pure will be adamantane left on the Si surface. The Pt interlayer on the Si substrate adsorbs the hydrocarbons from carbon source materials (adamantane), which can play a major role in diamond nucleation and growth. The nucleation and growth of diamond on the Pt/Si substrate will be discussed. Moreover, the rate of film growth in MPCVD with 1% methane (CH_4) in hydrogen (H_2) was 0.45 μm h^{-1}.

2. EXPERIMENTAL METHODS

The schematic diagram for the deposition of diamond on Pt/SiO_2/Si is shown in Figure 1. The synthesis processes of the diamond films on Pt/SiO_2/Si are described as follows: mirror-polished p-type (100) silicon wafers with dimensions of 1 × 1 cm^2 without any mechanical pretreatment were used as the substrates. The substrates were ultrasonically cleaned with acetone and alcohol for 10 min, respectively, and then dried with high-pressure nitrogen gas to remove any contamination particles left on the surface. The oxide layer prevented silicidation between Pt and Si; therefore, we did not use BOE solution to remove the native oxide (SiO_2) from the Si surface. Further, the platinum particles/film were coated on SiO_2/Si substrates by a sputtering process for 210 s and then again cleaned with acetone and alcohol for 10 min, respectively. The Pt particles were not uniformly distributed on the Si surface. The average thickness/size of Pt particles is ~50 nm. Further, adamantane was seeded on cleaned Pt/SiO_2/Si samples by an ultrasonic method. In this method, the solution was prepared by using (100 mg) adamantane + (5 mL) hexane and stirring for 1 min (the commercial adamantane powders with 99+% purity were obtained from Sigma-Aldrich Chemie GmbH (CAS: 281-23-2)). After manually stirring for 60 s at room temperature, the adamantane was fully dissolved into the hexane solvent and became a clear (colorless) solution. The Pt/SiO_2/Si samples were then immersed into the solution for 10 min of ultrasonication. After ultrasonication, the adamantane was seeded on the Pt/SiO_2/Si surface. We did not use any kind of process to dry the sample. Because the evaporation property of hexane is very high, hexane evaporated from the sample and

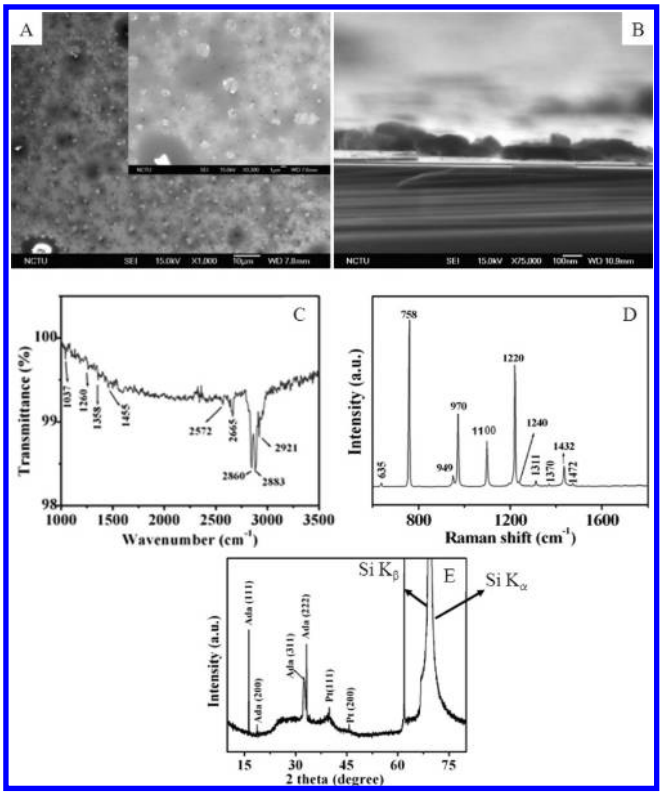

Figure 2. (A) Plan-view SEM image (inset is high-magnification image), (B) cross-sectional view, (C) FTIR spectrum, (D) Raman spectrum, and (E) X-ray diffraction pattern of adamantane on the Pt/SiO_2/Si after the ultrasonic process.

adamantane was left on the Pt/SiO_2/Si surface. Hexane is a colorless liquid, and it has considerable vapor pressure at room temperature. Hexane is relatively safe, largely unreactive, and easily evaporated. Finally, the adamantane-seeded Pt/SiO_2/Si substrates were then placed on a Mo-disk holder for diamond growth in a 1.5 AsTeX-type MPCVD system. The detailed processing parameters for MPCVD are as follows: the total pressure was 20 Torr, the microwave power was 600 W, the temperature was ≤700 °C, the total flow rate was 200 sccm (1% CH_4 in H_2), and the deposition time was varied from 2 to 120 min. The surface temperature was measured by an optical pyrometer. Finally, the samples were allowed to cool down to ambient temperature in the presence of hydrogen gas at 10 Torr. To know the role of Pt, we also prepared Si substrates without a Pt coating and treated with the same experimental conditions.

The surface morphology of the sample was examined using field-emission scanning electron microscopy (SEM, JEOL JSM-6700F), and the chemical composition of the surface was characterized by X-ray photoelectron spectroscopy (XPS, Thermo VG 350F, Mg K X-ray source). Elemental mapping in cross section was performed using a PHI700 scanning Auger nanoprobe (ULVAC-PHI Inc.). Examination of the internal microstructures of the deposited materials was carried out using transmission electron microscopy (TEM, Philips Tecnai20 operated at 200 kV). The cross-sectional TEM specimen was prepared using a focused ion beam (FIB, FEI Nova 200 dual-beam FIB). For the protection of the TEM specimen against damage from the high-energy ion beam (30 keV Ga+), the specimen was coated with platinum. Raman spectroscopy was

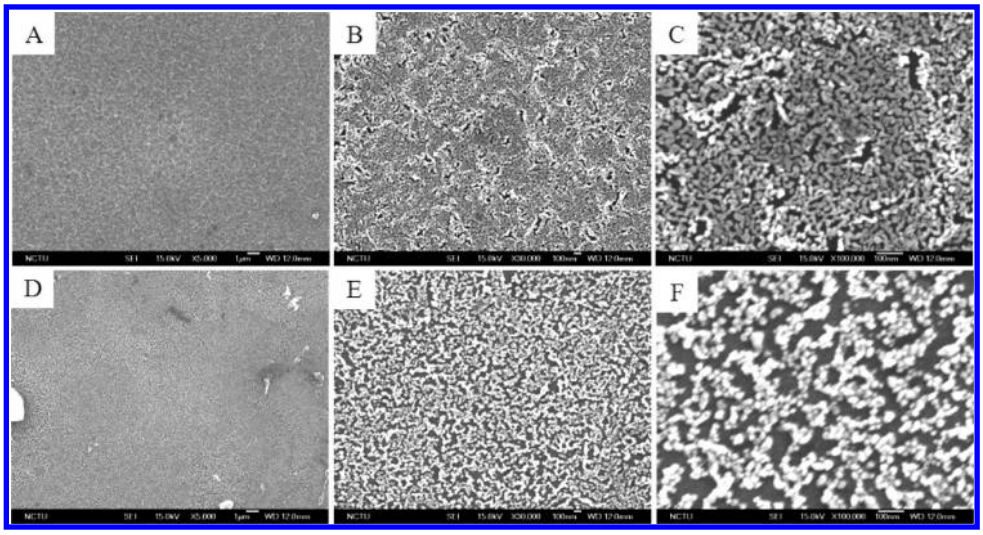

Figure 3. Top-view SEM images of (A−C) after 2 min and (D−F) after 5 min growth on adamantane/Pt/SiO_2/Si.

performed using a LABRAM HR800 system with an Ar laser (wavelength = 514.5 nm), which could be focused to a diameter of 1 mm for micromode operation. The crystallinity of the diamond was evaluated using an X-ray diffractometer (D2 XRD Bruker).

3. RESULTS AND DISCUSSION

After adamantane seeding on the Pt/SiO_2/Si surface by the ultrasonic treatment, the surface morphology was characterized by scanning electron microscopy (SEM). The plan-view SEM image is shown in Figure 2A. From the SEM image, it is clear that the adamantane particles are homogeneously dispersed on the Pt/SiO_2/Si surface by ultrasonic treatment. The inset high-magnification SEM image in Figure 2A shows that the adamantane particle sizes are varied from 10 nm to 1.5 μm. The cross-sectional SEM image in Figure 2B shows the thickness of adamantane particles. From the cross-sectional SEM image, it is clear that the adamantane particles ∼100 nm in thickness are deposited on the Pt/SiO_2/Si surface after 10 min of the ultrasonic process. Further, the bonding characteristics of the adamantane film were identified by Fourier transform infrared spectroscopy (FT-IR) and Raman spectroscopy, as shown in Figure 2C,D. There are several weak and strong peaks in Figure 2C. The peak at 1037 cm^{-1} was assigned to the CC stretch/CH bend, whereas the band at around 1107−1375 cm^{-1} was attributed to the sp^2 (C−H) group. In the FTIR spectrum, the peak due to CH_2 deformation appears as a strong absorption band at 1455 cm^{-1}. The strong band at 2572, 2665, 2860, 2883, and 2921 cm^{-1} was attributed to CH stretching.[19,20] In addition, the adamantane-seeded on the Pt/SiO_2/Si substrate was evaluated using Raman spectroscopy (LABRAM HR800). Intense Raman peaks in the range of 600−1800 cm^{-1} are shown in Figure 2D. All the multiple Raman peaks at 635, 758, 949, 970, 1095, 1220, 1240, 1311, 1432, and 1472, cm^{-1} are the typical characteristics of adamantane molecules.[21] We observed that the hydrocarbon signals from adamantane/Pt/SiO_2/Si are partially similar in the FTIR and Raman spectra, as shown in Figure 2C,D. We also noticed that there is not any kind of bond formation between adamantane and hexane. It is clear that the hexane is evaporated and only adamantane is left on the Pt/SiO_2/Si surface for diamond growth. In addition, we used D2 XRD to evaluate the adamantane/Pt/SiO_2/Si substrate. The XRD pattern in Figure 2E shows that the diffraction peaks at 2θ = 16.3, 18.8, 31.5, and 32.9° correspond to the interplanar spacings of adamantane {111}, {200}, {220}, {222}, and {640}, respectively. In addition to Si peaks, the diffraction peaks of Pt{111} and Pt{200} are seen at 39.8 and 46.3°, respectively,[22] indicating that Pt on the SiO_2/Si substrate has survived after the solution treatment of hexane and adamantane with ultrasonication.

After adamantane seeding on Pt/SiO_2/Si, we placed the sample in the MPCVD reactor for diamond growth. We used 1% CH_4 in H_2 for diamond growth. The growth time was varied from 2 to 15 min in the presence of 1% CH_4 in H_2. Figures 3 and 4 show the SEM images after different growth times. Plan-view SEM images in Figure 3A show that there is a homogeneously distributed film on the Pt/SiO_2/Si surface. The high-magnification SEM images in Figure 3B,C show that the film consists of networking islands. In general, a similar morphology has been observed in the carburization process for diamond nucleation and growth.[23] After 5 min of deposition, the shape of the particles are changed, as shown in Figure 3D−F, into the disconnected clusters with a density of $\sim 10^{11-12}$ cm^{-2}. After 10 min of deposition, the SEM images in Figure 4A−C show that most of the particles are formed in the spherical shape with an average size of less than 100 nm. The SEM image in Figure 4F shows that some oriented carbon particles in square and triangle shapes have been formed after 15 min growth. The density of the carbon particles is $\sim 10^{7-8}$ cm^{-2}.

Further, the cross-sectional SEM images after 2, 5, 10, and 15 min of deposition are shown in Figure 5. After 2 min of deposition, the film thickness is ∼100 nm, similar to that of the adamantane seeding film, suggesting that most of the fractions of adamantane molecules may have undergone a transformation into other forms of carbon species in MPCVD as no adamantane evidence can be obtained from Raman data shown later. After 5 and 10 min of deposition, the average particle height is ∼115 and 130 nm, whereas it is ∼150 nm after 15 min. It is clear that the height increases with the deposition time.

In addition, we used Auger electron mapping in cross section to identify the presence of elements and their distribution on the surface after 2 min of treatment. The elemental mapping in cross section was performed in a PHI 700 scanning auger nanoprobe

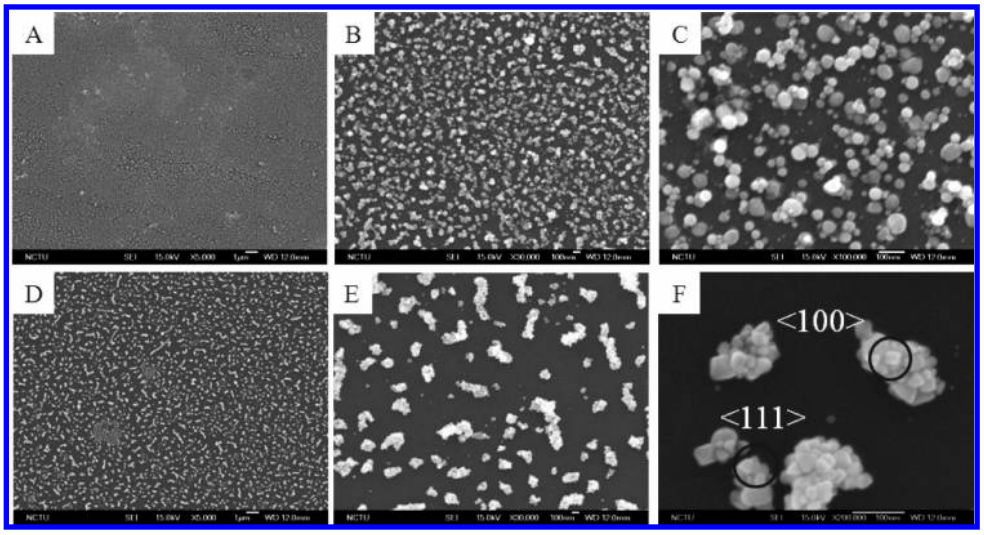

Figure 4. Top-view SEM images of (A−C) after 10 min and (D−F) after 15 min growth on adamantane/Pt/SiO_2/Si.

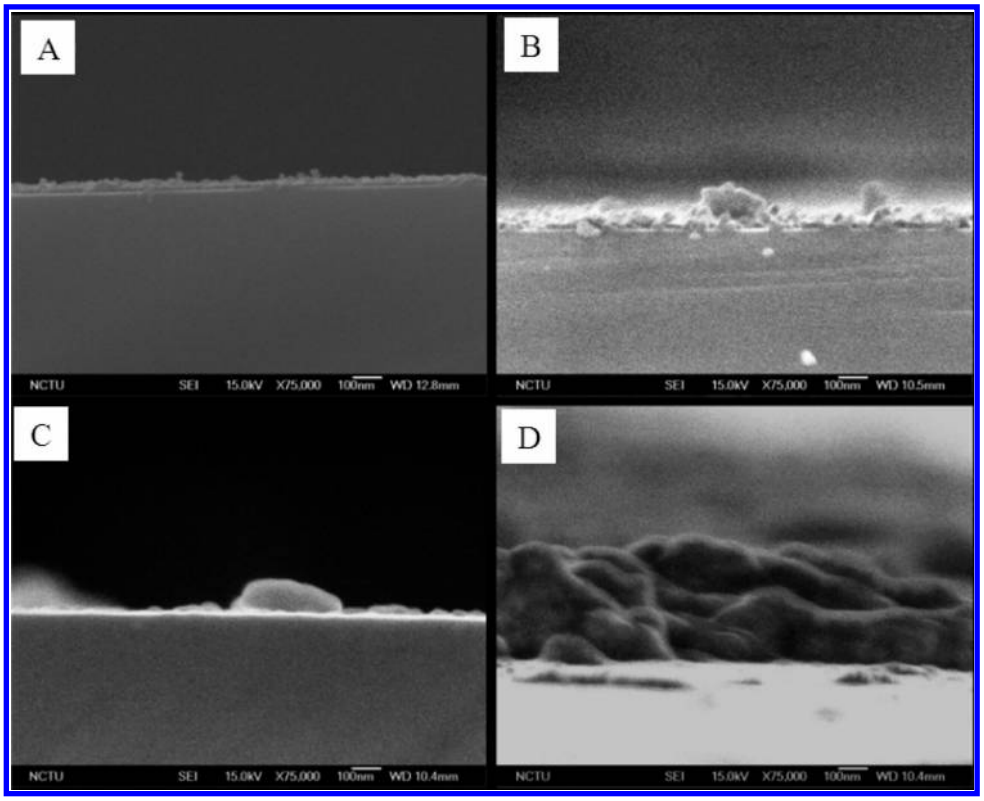

Figure 5. Cross-sectional view SEM images of (A) after 2 min, (B) after 5 min, (C) after 10 min, and (D) after 15 min growth on adamantane/Pt/SiO_2/Si.

(ULVAC-PHI Inc.). The cross-sectional specimen was prepared simply by cleavage. Figure 6A shows an SEM micrograph in cross-sectional view with the corresponding maps of C, Pt, and Si in Figure 6B−D. From the image contrast in SEM and the elemental maps, one can clearly identify two regions that correspond to carbon and Si phases, while the Pt interlayer shows low contrast. There are two possibilities to show low contrast: (i) the platinum particles were not uniformly distributed on the surface and (ii) the Pt may overlap with hydrocarbons. Moreover, to understand the role of the Pt interlayer in diamond deposition, we prepared adamantane-coated samples on SiO_2/Si substrates without the Pt coating under the same experimental conditions. After 2 min of deposition, we can see that the carbon film is not uniformly distributed on the Si surface, as shown in Figure 7A. It is likely that most of the fractions of adamantane are either etched by hydrogen plasma or evaporated. The high-magnification SEM image (Figure 7B) shows that the particles are several nanometer sizes. After 5, 10, and 15 min of deposition, particles are uniformly distributed. The sizes of the carbon particles are changed with deposition time. In comparison, the

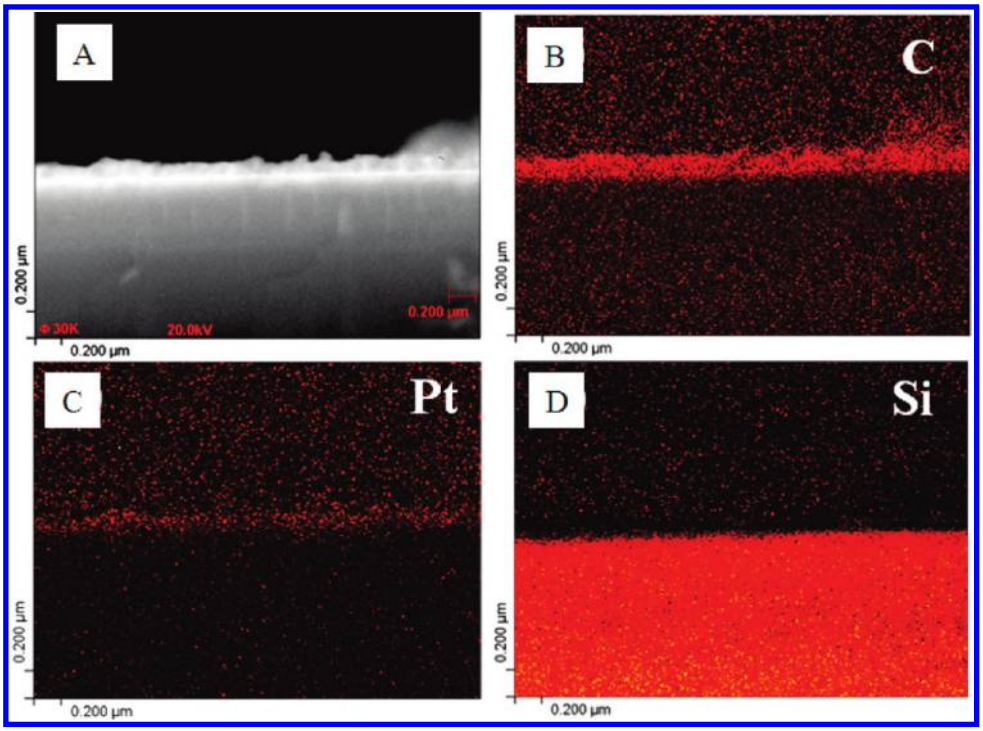

Figure 6. (a) Cross-sectional SEM of deposited adamantane/Pt/Si with the corresponding nanobeam Auger electron mapping of (b) carbon, (c) platinum, and (d) silicon.

density of particles became less in the absence of the Pt interlayer. Furthermore, the samples after deposition on adamantane seeded on $Pt/SiO_2/Si$ and without Pt (adamantane seeded/Si) were characterized by Raman spectroscopy, as shown in Figure 8. In both cases, similar features are observed [broad range (1250−1370 cm^{-1}) and G band]. The broad range peak (1250−1370 cm^{-1}) shows the presence of sp^2/sp^3. In the broad peak range (1250−1370 cm^{-1}), we observed the high-intensity peak at 1325 and 1327 cm^{-1} along with the G band in both cases (after 15 min of deposition), as shown in Figure 8A,B. Previous studies have shown that these peaks (1325 and 1327 cm^{-1} in both cases) show the presence of a nanodiamond phase and the peak shifting due to the effect of the nanodiamond size.[24] On the other hand, the second-order G band does not require an elastic defect-related scattering process and has been shown for defect-free sp^2 carbons.[25] Figure 8 shows that the intensity of peaks is increasing with deposition times. If the bands (D and G) have similar intensities, this may imply a high quantity of structural defects.[25,26] Up to 10 min, the intensity of Raman signals is almost similar in both cases. However, we noticed that the one additional peak (presence of Pt) at 1339 cm^{-1} corresponds to diamond. After 15 min (Figure 8A), a sharp Raman peak at 1598 cm^{-1} is observed. However, we did not notice any such kind of peak in the case of without Pt (Figure 8B). Therefore, it is likely that more graphite particles or other sp^2 phases along with the nanodiamond (sp^3) phase formed in the presence of the Pt interlayer than without Pt. The weak Raman signals at 1480, 1519, 1416, 1441, and 1716 cm^{-1} come from different carbon phase. Previously we reported that the Raman peak at 1480 cm^{-1} may come from nanodiamond. Therefore, it is possible that, in a short deposition time (2 min), some nanodiamond (sp^3) may form on Pt, and further deposition results in the change of the sp^3 phase to other carbon phases.

It is well known that pure hydrogen plasma can etch the hydrocarbon layer. Therefore, to evaluate the adsorption of hydrocarbon by Pt, we prepared two adamantane seeded on $Pt/SiO_2/Si$ samples that were treated with pure hydrogen gas plasma for 5 and 15 min, as shown in Figure 9. The SEM image in Figure 9A shows that the carbon film (after 5 min of etching) was uniformly distributed on the $Pt/SiO_2/Si$ surface. The high-magnification SEM image in Figure 9B shows the surface morphology of carbon film, which formed a network structure after 5 min of treatment. After 15 min of treatment, the carbon network is broken by hydrogen plasma (Figure 9D). However, when we treated adamantane/Si (without Pt) with pure hydrogen plasma at the same experimental condition, most of the film disappeared and few particles were left on the Si surface. Therefore, it strongly suggests that the Pt particles/interlayer can effectively adsorb the hydrocarbons and significantly reduce the evaporation rate of adamantane (hydrocarbon) from the surface,[27] which then might transform into other forms of carbon phases.

In addition, XPS was used to identify the presence of chemical compositions on $Pt/SiO_2/Si$ surface after 2, 5, 10, and 15 min depositions. Figure 10A shows the survey spectrum of adamantane seeded on $Pt/SiO_2/Si$ treated with 1% CH_4 in H_2 for various times (2, 5, 10, and 15 min), whereas Figure 11A shows the survey spectrum of adamantane seeded on $Pt/SiO_2/Si$ treated (5 min) with pure hydrogen (200 sccm). In addition to XPS signals due to Pt particles/film and the carbon overlayer, the XPS analysis also detected O(1s), Si(2p), and Si(2s) photoelectrons in both cases (Figures 10A and 11A). The XPS high-resolution spectra of carbon (C 1s) is shown in Figure 10B−E. It is reasonable to expect that the adamantane composed into CH_x species after various time treatments (2, 5, 10, and 15 min). Each of the fitting components is almost similar in all cases. The

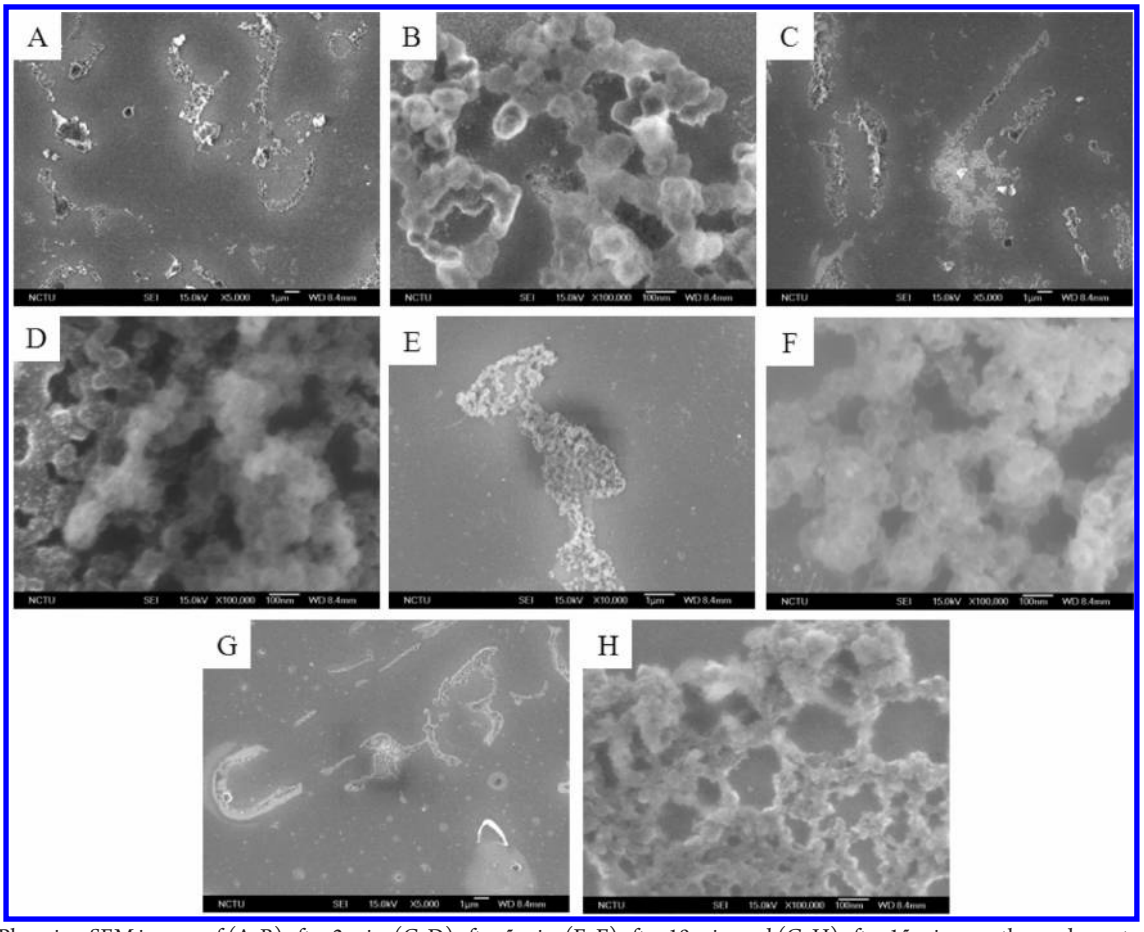

Figure 7. Plan-view SEM images of (A, B) after 2 min, (C, D) after 5 min, (E, F) after 10 min, and (G, H) after 15 min growth on adamantane/SiO_2/Si (without Pt).

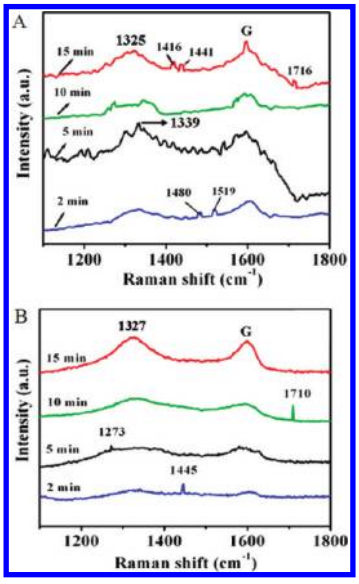

Figure 8. Raman spectra of (a) adamantane seeded Pt/SiO_2/Si (with Pt) and (b) adamantane seeded SiO_2/Si (without Pt) after 2, 5, 10, and 15 min treated with 1% CH_4 in H_2 at the same experimental conditions.

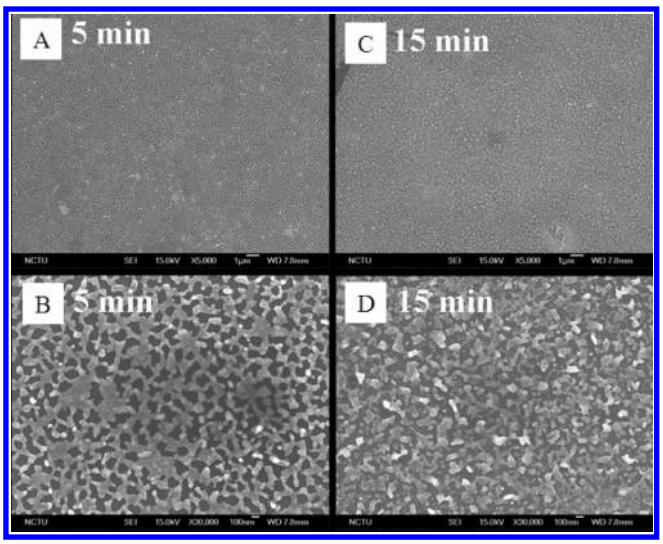

Figure 9. Plan-view SEM images of (a, b) after 5 min and (c, d) after 15 min, treated with pure hydrogen plasma on adamantane/Pt/SiO_2/Si.

carbon (C 1s) was assigned as follows: sp^3 carbon with C−C bonds (C−C sp^3 carbon, 283.7−283.8 eV), sp^2 carbon with C−C bonds (C−C sp^2 carbon, 284.4−284.45 eV), sp^2 carbon with H−C bonds (H−C sp^2 carbon, 284.8 eV), sp^3 carbon with H−C bonds (H−C sp^3 carbon, 285.2−285.3 eV), and CO at ∼287.1 and 287.7 eV.[28,29] Interestingly, the carbon signals from the pure hydrogen-treated sample (after 5 min) in Figure 11B shows the doublet peaks of carbon at 284.5 and 287.6 eV. The

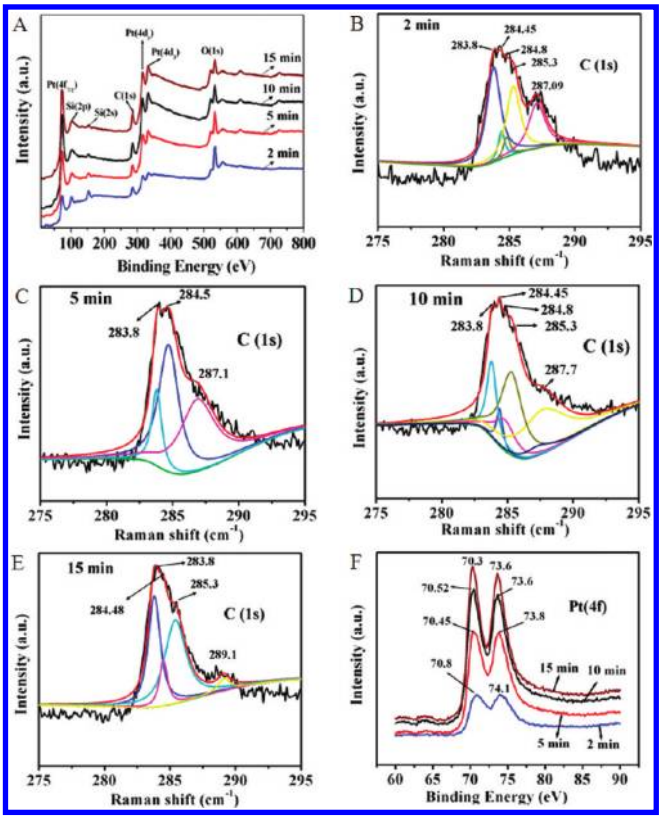

Figure 10. XPS spectra: (A) survey spectra, (B−E) high-resolution spectra of the C (1s), and (F) high-resolution spectra of the Pt (4f) region of adamantane/Pt/SiO_2/Si after various treatment times.

peak is approximately at 284.5 eV, which is the typical characteristics of graphite sp^2 bonding.[30,31] The signal at 284.5 eV shows the presence of the graphite phase, while 287.6 eV is from carbonyl or C−O groups.[29] The XPS carbon signal at 289.1 eV also corresponds to carbonyl or C−O groups.[32] It is most likely that carbon bonded with native layer oxygen (SiO_2). Similar observations are seen in the spectra for the cases of deposition with CH_4, as shown in Figure 10B−E. Figure 10B−E shows that the intensity of the carbon peak is increasing with treatment times. Therefore, the surface concentration of the carbon (sp^2) phase may increase with deposition time. Nevertheless, the sp^3 carbon might be always present on the surface in all cases. In previous studies, Han et al. and Lambrecht et al. have shown that graphitic carbon is an effective precursor for diamond nucleation.[33,34] Kompoulos et al. and Feng et al. have noticed diamond film on the thin amorphous carbon-coated Si substrate, while Barnes et al. had noticed the high density of diamond nucleation on the Si substrate, which was first scratched with diamond paste and then deposited with a non-diamond amorphous carbon film.[35−37]

The Pt(4f) XPS spectrum shown in Figures 10F and 11C exhibited a broad doublet peak with the Pt($4f_{7/2}$) peak maximum at 70.3 eV, which negatively shifted from that for bulk Pt by∼0.9 eV. We ascribe the negative binding energy shift of the Pt(4f) doublet peak to the size effect of Pt particles. The oxygen signal at 532.7 eV is associated with native oxide on the Si surface. The oxygen peak at 532.7 eV is attributed to the O−Si bond in SiO_2.[38,39] The signals of silicon Si(2p) and Si(2s) at 99 and 151 eV indicate that the substrate surface is uncovered by Pt and carbon films.[40]

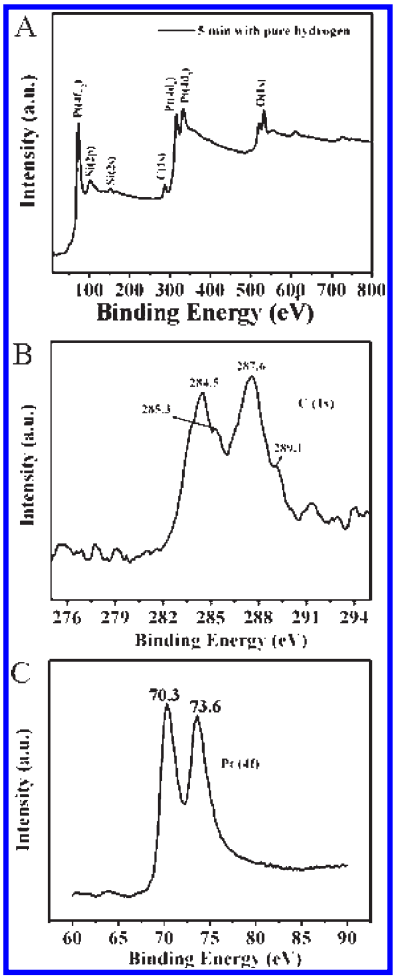

Figure 11. (A) XPS survey spectrum of adamantane/Pt/SiO_2/Si, (B) high-resolution spectrum of the C (1s), and (C) high-resolution spectrum of the Pt (4f) region after 5 min of treatment with pure hydrogen plasma.

Diamond Formation after 120 min Deposition Time. Further, diamond growth for 120 min was carried out on adamantane-seeded Pt/SiO_2/Si substrates and adamantane-seeded SiO_2/Si substrates without the Pt overcoating. The structure and surface morphology of synthesized diamond and their characteristics are shown in Figure 12. Figure 12A−C shows the SEM images of the deposition on Pt/SiO_2/Si, revealing that the diamonds have been synthesized uniformly on the Pt/SiO_2/Si substrate in a cauliflower shape with the appearance of some {100} diamond facets. For the sample without the Pt interlayer, the synthesized diamonds in the {100} facet are clearly seen in Figure 12D. However, the density of diamond in the sample with the Pt interlayer is $\sim 10^8$ cm^{-2}, much higher than 10^6 cm^{-2} on that without the Pt interlayer, as shown in Figure 12A,D. Thus, it is clear that the coating of adamantane on the Pt interlayer can enhance the diamond density. The thickness of diamond on Pt/Si is ∼900 nm, as shown in Figure 12C, giving the growth rate of diamond of ∼0.45 μm/h. In addition, the XRD pattern supports the formation of the microcrystalline diamond film on Pt/SiO_2/Si, as shown in Figure 12E. In addition to Si peaks, the XRD pattern in Figure 12E presents sharp and well-defined peaks at 2θ = 39.8, 43.9, 44.6, and 46.39° corresponding to the interplanar spacings of Pt {111}, diamond {111}, graphite {101}, and Pt {200}, respectively.

dx.doi.org/10.1021/jp2041179 |J. Phys. Chem. C 2011, 115, 16063–16073

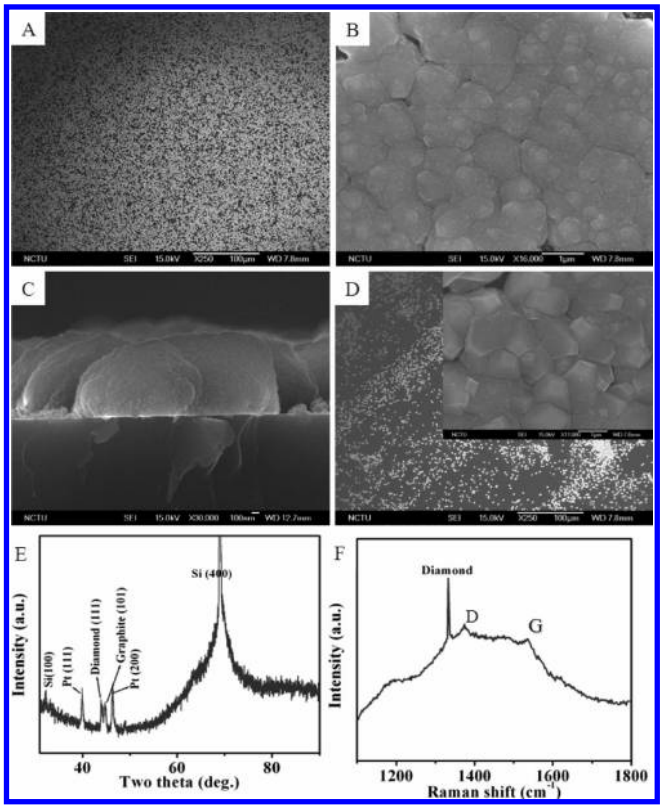

Figure 12. (A) Plan-view SEM, (B) high-magnification SEM image, (C) cross-sectional SEM image of diamond (growth time, 2 h) on Pt/SiO_2/Si, (D) plan-view (the inset shows a high-magnification image of diamond on substrate without Pt), (E) XRD pattern, and (F) Raman spectra of diamond (growth time, 2 h) on Pt/SiO_2/Si.

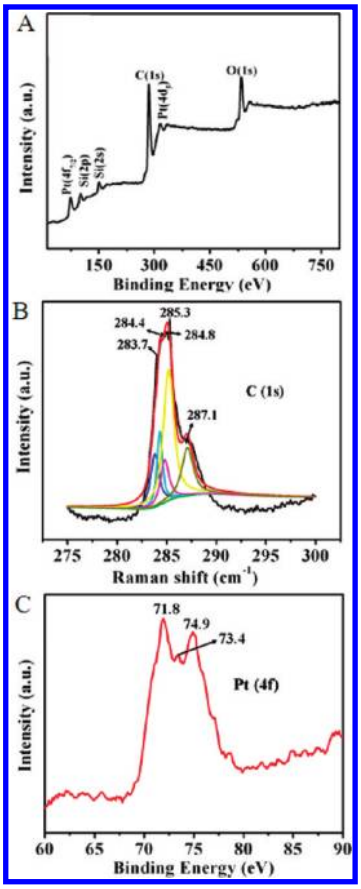

Figure 13. XPS spectra: (A) survey spectrum, (B) high-resolution spectrum of the C (1s), and (C) high-resolution spectrum of the Pt (4f) region of diamond on adamantane/Pt/SiO_2/Si.

Moreover, the micro-Raman spectrum of the diamond film on Pt/SiO_2/Si is shown in Figure 12F. The characteristic feature of diamond at 1332 cm^{-1} is clearly observed, the full width at half-maximum of the peak is determined to be 7.2 cm^{-1}. The film also contains disordered graphitic carbon components or amorphous carbon, as indicated by D and G bands. We also used XPS to characterize the diamond Pt/SiO_2/Si, as shown in the survey spectrum of Figure 13A. Apart from the expected peaks from elements of diamond (C) and Pt, the oxygen signal has also been detected. Figure 13B shows the XPS C(1s) spectrum of the diamond sample. The deconvolution of the spectrum has shown that the C 1s peaks are composed of three peaks at ~283.7−284.4, 284.8, 285.3, and 287.1 eV corresponding to C−C (sp^3), C−C and C−H (sp^2), and C−O bondings.[31−43] The negative binding energy (0.5 eV) shift, as shown in the high-resolution spectrum of Pt(4f) (Figure 13C), is due to the size effect of Pt particles. However, the Pt(4f) peak at 73.4 eV corresponds to Pt−C bonding.[44]

Furthermore, the cross-sectional TEM specimen of a sample (adamantane seeded on Pt/SiO_2/Si) deposited for 2 h was prepared by the focused ion beam (FEI Nova 200 Dual beam FIB). For the protection of the TEM specimen against damage from the high-energy ion beam (30 keV Ga^+) in FIB, the specimen was coated with platinum. A cross-sectional bright-field TEM image of diamond/Pt/SiO_2/Si is shown in Figure 14A. From Figure 14A, the dark contrast regions are actually corresponding Pt particles (as shown in the following EDX) with a size of ~5 to ~50 nm. Clearly, the Pt is not a continuous interlayer. Also, it is seen that the thickness of the diamond particle is ~900 nm. The HRTEM image in Figure 14B is obtained from an interfacial region without the Pt particles, showing diamond and Si lattice fringes. The inset fast Fourier transform (FFT) of the lattice image of Si and diamond shows the diffraction characteristics from which the measured interplanar spacing of ~2.06 Å can be identified to be the diamond {111} one (Figure 14B). Between diamond and Si, it shows amorphous SiO_2 with a thickness of ~4 nm. The SAD pattern obtained from around the marked region of the particle (Figure 14B) shows the single crystalline diamond characteristics in the ⟨110⟩ zone axis. To further identify the Pt phase at the interface, we acquired EDX from different regions, as shown by the numbers in Figure 14A. In Figure 15, the EDX spectrum from region 1 (Figure 14A), where we can see some particles (in black contrast) at the interface, shows Pt, Si, and O peaks, whereas at region 2 on the interface (where no black particles exist), it shows Si, O, and Cu peaks. Therefore, it is clear that the Pt signal comes from black particles, while O and Si signals are from SiO_2 on Si substrate. The Cu signal comes from the Cu grid. The EDX from region 3 (from Si substrate) shows the Si and O, and that from region 4 (diamond particles) shows the high concentration of carbon. It is also clear that the SiO_2 layer between Pt and Si prevents the silicidation. Hayashi et al have observed high crystalline (111) oriented diamond on Pt/TiO_2/SiO_x/Si. The oxide layers prevented the silicidation formation between Pt and Si, and it may also prevent the formation of SiC.

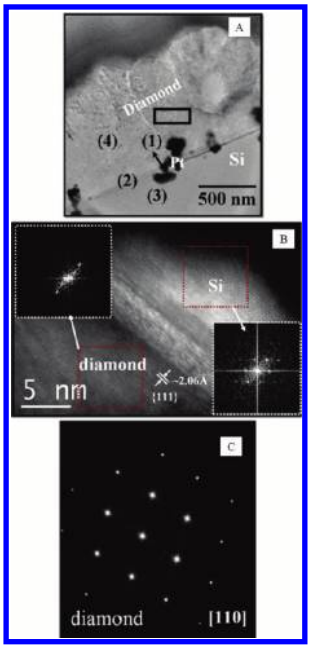

Figure 14. (A) Cross-sectional BF-TEM image of diamond/Pt/Si. (B) HRTEM image of diamond/Si. The *d*-spacing between the fringes was ~2.06 Å of the diamond {111} plane. The insets show FFT patterns of Si and diamond lattice images (indicated by arrow). (C) SAED from marked (rectangle) region of diamond along the ⟨110⟩ direction.

The schematic diagram of the growth of diamond film on the $Pt/SiO_2/Si$ substrate is shown Figure 16. The bonding characteristics depend on their structure, such as saturated hydrocarbons, which are weakly adsorbed. Methane can desorb intact from the Pt (111) surface by heating.[45] Unsaturated hydrocarbons can make covalent bonds with the Pt surface. Jacob et al. have shown adsorption of various CH_x and C_2H_y hydrocarbons with the Pt surface. They noticed that, in each case, the structures on the surface are comparable to gas-phase analogues in which some CH bonds are replaced with C−Pt *ó* bonds.[45] The hydrogen is highly soluble in transition metals. Therefore, we predicate that, during ultrasonication, adamantane would have been adsorbed on the $Pt/SiO_2/Si$ surface. In the CVD, the hydrocarbon radicals from the plasma (1% CH_4 in H_2 plasma) with the seeded adamantane might form the Pt−C−H complex. Hydrogen ions ($H^{\pm}$, $H_2^{\pm}$, $H_3^{\pm}$) in H/C plasma (1% CH_4/H_2 mixture in mw plasma CVD reactor) are converted into hydrocarbon ions, $C_xH_y^{\pm}$, in ion conversion reactions and concentrations $[H_x^{\pm}] \ll [C_xH_y^{\pm}]$[46] as a result; the effect of hydrogen ions seems to be negligible in comparison with $C_xH_y^{\pm}$ ions. From the C 1s signals in XPS spectra (Figures 10, 11, and 13), it is shown that the CO bond is present on the surface. It seems that Pt behaves as a catalyst and support to CO bond formation in early stage (2 min) deposition, as shown in Figure 10B. Therefore, CO bonding can overcome the evaporation rate of adamantane and enhance the density. In general, hexane has evaporation properties. However, Pt adsorbs the hydrocarbons; therefore, a chemical reaction not only has taken place with adamantane but also may have taken place with hexane (C_6H_{14}). Previous studies have shown that the hexane can react with Pt.[47] The melting point of Pt (~1772 °C) is much higher than the growth temperatures used in this study. The solid solubility of C in Pt is less than 1 atom % at 650 °C according to the Pt−C binary phase diagram.[48]

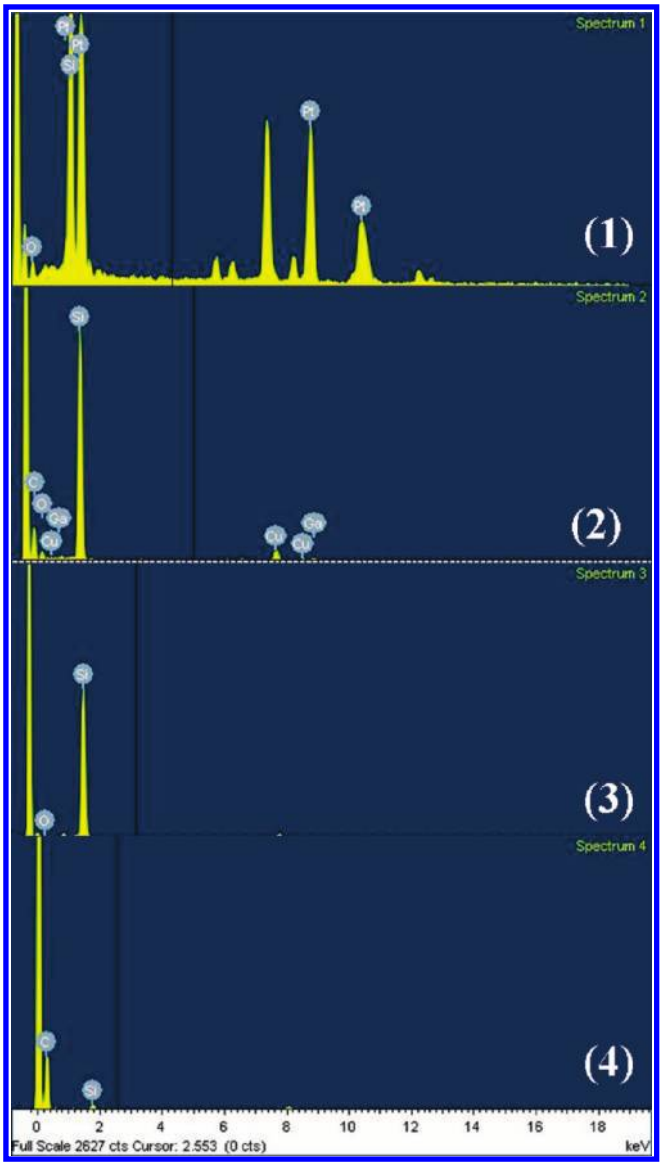

Figure 15. EDX spectra of inset mark in BF image in Figure 14A: (1) from Pt interface particles, (2) without Pt particles in the interfacial region, (3) Si substrate, and (4) from diamond particles.

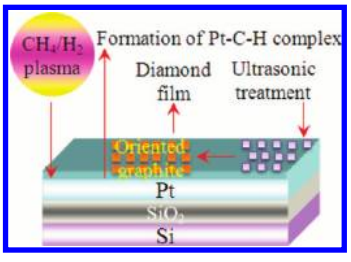

Figure 16. Schematic diagram of diamond growth on adamantane seeded on $Pt/SiO_2/Si$ substrates.

Therefore, it is unlikely that the dissolution medium is a pure form of Pt or a Pt−C solid solution. It is rather appropriate to consider the Pt−C−H ternary system in order to understand the SEM observations as the present CVD growth of diamond was

conducted in a predominantly hydrogen plasma environment. Hydrogen in its atomic form has a small atomic radius, easily dissolves in Pt, and would weaken the bond strength and lower the effective melting point of the ternary system. Roy and co-workers claimed the importance of the metal−C−H systems in their observation of diamond growth from Ni−C and Cu−C mixtures in hydrogen plasma.[49] After 15 min of treatment, the adsorbed Pt−C−H complex may promote the formation of some carbon particles, which then act as nuclei for growth of diamond film in the presence of CVD plasma (1% CH_4 in H_2 plasma).

4. CONCLUSIONS

We have confirmed that diamond films are successfully grown on adamantane-seeded Pt/SiO_2/Si substrates by MPCVD from the gaseous mixture of methane and hydrogen. The seeded adamantane was first transformed into nanodiamond and some unidentified carbon particles in the early stage of deposition within 2 min. After further deposition of 5−15 min, the existence of the graphite phase is evident, while no adamantane and nonodiamond can be identified. With a long time deposition of 120 min, diamond formation is observed. The SiO_2 layer between Pt and Si not only prevents the silicidation reaction but also avoids the formation of silicon carbide. The density of synthesized diamond on Pt/SiO_2/Si was higher than that without Pt/SiO_2/Si.

AUTHOR INFORMATION

Corresponding Author

*E-mail: rajanisht@gmail.com.

ACKNOWLEDGMENT

The authors would like to thank the National Science Council of the Republic of China, Taiwan, for financially supporting this research under contract NSC96-2622-E-009-002-CC3 and 98-2221-E-009-042-MY3.

REFERENCES

(1) Dearnaley, G.; Arps, J. H. *Surf. Coat. Technol.* **2005**, *200*, 2518–2524.
(2) Yan, J. K.; Chang, L. *Nanotechnology* **2006**, *17*, 5544–5548.
(3) Chen, H. G.; Chang, L. *Diamond Relat. Mater.* **2009**, *18*, 141–145.
(4) You, M. S.; Hong, F. C. N.; Jeng, Y. R.; Huang, S. M. *Diamond Relat. Mater.* **2009**, *18*, 155–159.
(5) Walkowiak, B.; Okroj, W.; Jerczynska, H.; Pawlowska, Z. *Diamond Relat. Mater.* **2009**, *18*, 651–656.
(6) Wolter, S. D.; McClure, M. T.; Glass, J. T.; Stoner, B. R. *Appl. Phys. Lett.* **1995**, *66*, 2810–2812.
(7) Tiwari, R. N.; Chen, W.-C.; Wang, W.-L.; Chang, L. *J. Appl. Crystallogr.* **2010**, *43*, 883–889.
(8) Saito, T.; Tsuruga, S.; Ohya, N.; Kusakabe, K.; Morooka, S.; Maeda, H.; Sawabe, A.; Suzuki, K. *Diamond Relat. Mater.* **1998**, *7*, 1381–1384.
(9) Tachibana, T.; Yokota, Y.; Hayashi, K.; Miyata, K.; Kobashi, K.; Shintani, Y. *Diamond Relat. Mater.* **2000**, *9*, 251–255.
(10) Tachibana, T.; Yokota, Y.; Miyata, K.; Kobashi, K.; Shintani, Y. *Diamond Relat. Mater.* **1997**, *6*, 266–271.
(11) Shintani, Y. *J. Mater. Res.* **1996**, *11*, 2955–1956.
(12) Tachibana, T.; Yokota, Y.; Miyata, K.; Onishi, T.; Kobashi, K.; Tarutani, M.; Takai, Y.; Shimizu, R.; Shintani, Y. *Phys. Rev. B* **1997**, *56*, 15967–15981.
(13) Hayashi, Y.; Matsushita, Y.; Soga, T.; Umeno, M.; Jimbo, T. *Diamond Relat. Mater.* **2002**, *11*, 499–503.
(14) Tiwari, R. N.; Tiwari, J. N.; Chang, L. *Chem. Eng. J.* **2010**, *158*, 641–645.
(15) Tiwari, R. N.; Chang, L. *J. Appl. Phys.* **2010**, *107*, 103305.
(16) Tiwari, J. N.; Tiwari, R. N.; Chang, Y. M.; Lin, K. L. *ChemSusChem* **2010**, *3*, 460–466.
(17) Umeno, M.; Noda, M.; Uchida, H.; Takeuchi, H. *Diamond Relat. Mater.* **2008**, *17*, 684–687.
(18) Tiwari, R. N.; Chang, L. *Appl. Phys. Express* **2010**, *3*, 045501.
(19) Oomens, J.; Polfer, N.; Pirali, O.; Ueno, Y.; Maboudian, R.; May, P. W.; Filik, J.; Dahl, J. E.; Liu, S.; Carlson, R. M. K. *J. Mol. Spectrosc.* **2006**, *238*, 158–167.
(20) Corn, R. M.; Shannon, V. L.; Synder, R. G.; Strauss, H. L. *J. Chem. Phys.* **1984**, *81*, 5231–5238.
(21) Filik, J.; Harvey, J. N.; Allan, N. L.; May, P. W.; Dahl, J. E. P.; Liu, S.; Carlson, R. M. K. *Spectrochim. Acta, Part A* **2006**, *64*, 681–692.
(22) Zheng, T.; Nishiyama, N.; Egashira, Y.; Ueyama, K. *Stud. Surf. Sci. Catal.* **2006**, *162*, 561–567.
(23) Tarakci, M.; Korkmaz, K.; Gencer, Y.; Usta, M. *Surf. Coat. Technol.* **2005**, *199*, 205–212.
(24) Sun, K. W.; Wang, C. Y. *J. Phys.: Conf. Ser.* **2007**, *92*, 012031.
(25) Costa, S.; Palen, E. B.; Kruszynska, M.; Bachmatiuk, A.; Kalenczuk, R. J. *Mater. Sci.-Pol.* **2008**, *2*, 433–441.
(26) Scheibe, B.; Palen, E. B.; Kalenczuk, R. J. *Mater. Charact.* **2010**, *61*, 185–191.
(27) Kobashi, K. *Diamond Films: Chemical Vapor Deposition for Oriented and Heteroepitaxial Growth*; Elsevier Science: Amsterdam, 2005.
(28) Takabayashi, S.; Okamoto, K.; Shimada, K.; Motomitsu, K.; Motoyama, H.; Nakatani, T.; Sakaue, H.; Suzuki, H.; Takahagi, T. *Jpn. J. Appl. Phys.* **2008**, *47*, 3376–3379.
(29) Dagli, G.; Sung, N.-H. *Polym. Compos.* **1989**, *10*, 109–116.
(30) Smirnova, T. P.; Badalyan, A. M.; Borisov, V. O.; Yakovkina, L. V.; Kaichev, V. V.; Shmakov, A. N.; Nartova, A. V.; Rakhlin, V. I.; Fomina, A. N. *High Energy Chem.* **2003**, *37*, 303–309.
(31) Kvon, R. I.; Boronin, A. I.; Shaikhutdinov, S. K.; Buyanov, R. A. *Appl. Surf. Sci.* **1997**, *120*, 239–242.
(32) Delamar, M.; Dbsarmot, G.; Fagebaume, O.; Hitmi, R.; Pinson, J. *Carbon* **1997**, *35*, 801–807.
(33) Han, Y. X.; Ling, H.; Sun, J.; Zhao, M.; Gebre, T.; Lu, Y. F. *Appl. Surf. Sci.* **2008**, *254*, 2054–2058.
(34) Lambrecht, W. R. L; Lee, C. H.; Segall, B.; Angus, J. C.; Li, Z.; Sunkara, M. *Nature* **1993**, *364*, 607–610.
(35) Komvopoulos, K.; Xu, T. *Diamond Relat. Mater.* **2000**, *9*, 274–282.
(36) Feng, Z.; Komvopoulos, K.; Bogy, D. B.; Ager, J. W.; Anders, S.; Anders, A.; Wang, Z.; Brown, I. G. *J. Appl. Phys.* **1996**, *79*, 485.
(37) Barnes, P. N.; Wu, R. L. C. *Appl. Phys. Lett.* **1993**, *62*, 37–39.
(38) Schaller, E. M.; Kuettel, O. M.; Schlapbach, L. *Phys. Status Solidi A* **1996**, *153*, 415–429.
(39) Gsell, S.; Berner, S.; Brugger, T.; Schreck, M.; Brescia, R.; Fischer, M.; Greber, T.; Osterwalder, J.; Stritzker, B. *Diamond Relat. Mater.* **2008**, *17*, 1029–1034.
(40) Boukherroub, R.; Wayner, D. D. M.; Sproule, G. I.; Lockwood, D. J.; Canham, L. T. *Nano Lett.* **2001**, *1*, 713–717.
(41) Saw, K. G.; du Plessis, J. *Mater. Lett.* **2004**, *58*, 1344–1348.
(42) Ong, S.-E.; Zhang, S.; Du, H.; Sun, D. *Diamond Relat. Mater.* **2007**, *16*, 1628–1635.
(43) Ahmed, M.; Byrne, J. A.; McLaughlin, J. A. D. *e-J. Surf. Sci. Nanotechnol.* **2009**, *7*, 217–224.
(44) Parravano, G. *J. Catal.* **1970**, *16*, 1–15.
(45) Jacob, T.; Goddard, W. A., III *J. Phys. Chem. B* **2005**, *109*, 297–311.
(46) Mankelevich, Y. A.; Ashfold, M. N. R.; Ma, J. *J. Appl. Phys.* **2008**, *104*, 113304.
(47) Matusek, K.; Paal, Z. *React. Kinet. Catal. Lett.* **1999**, *67*, 241–246.

(48) Massalski, T. B.; Okamoto, H.; Subramanian, P. R.; Kacprzak, L., Eds.; *Binary Alloy Phase Diagrams*; ASM International: Materials Park, OH, 1990; p 794.
(49) Roy, R.; Dewan, H. S.; Ravindranathan, P. *Mater. Res. Bull.* **1993**, *28*, 861–866.